Freeform 3D Printing of Soft Hydrogel Electronics

Yue Hui
Westlake University
Qilin Qian
Westlake University https://orcid.org/0000-0002-6049-0051
Yuan Yao
Westlake University
Hehao Chen
Westlake University
Zheng Qiao
National University of Singapore
Yetian Yu
Westlake University
Nanjia Zhou (zhounanjia@westlake.edu.cn)
Westlake University

Article

Keywords:

Posted Date: February 2nd, 2022

DOI: https://doi.org/10.21203/rs.3.rs-1080224/v1

Version of Record: A version of this preprint was published at Nature Electronics on December 19th, 2022.
See the published version at https://doi.org/10.1038/s41928-022-00887-8.

Abstract

Soft electronics have attracted enormous attentions in the growing field of bioelectronic integration. Among the various material choices, hydrogels are of particular interest due to their intrinsic similarities with biological tissues. However, challenges still remain for the fabrication of hydrogel electronics, especially those featuring 3D form-factors to conform with the complex biological environment. Here we develop a set of materials which allows for the first time, fully 3D printing of soft electronics featuring soft circuits with arbitrary form factors embedded within soft hydrogel matrix. We design an embedded 3D printing (EM3DP) technology with a curable, ultra-soft (< 5 kPa) and stretchable ($\lambda \sim 18$) hydrogel matrix by employing packed hydrogel microparticles possessing a secondary crosslinking capability, and a highly conductive (~1.4×10^3 S/cm) Ag–hydrogel composite with a segregated conductive network structure. We fabricate various hydrogel-based passive electronics and demonstrate their functionalities. Furthermore, discrete surface-mount components can be readily picked-and-placed at any pre-determined position within the hydrogel matrix and connected with printed passive structures through a highly automated process, thereby greatly expanding the soft electronic functionalities. This work demonstrates the versatility of EM3DP for the future manufacturing of hydrogel-based 3D electronics.

Introduction

The growing demand on advanced healthcare has prompted the advent of numerous applications at the bio-electronic interfaces, ranging from wearable/epidermal devices to implantable electronics,[1–4] with diverse functionalities including bio-signal detection,[2,5] health monitoring[6,7], and nerve stimulation,[8,9] etc. To gain closer insights into brain science, regenerative medicine and developmental biology, considerable efforts have also been dedicated to the investigation of brain–computer interface,[10] neuromuscular junctions[11], and even cyborg tissues,[3,12] spurring the development of new materials and manufacturing methods for soft electronics to meet the requirements of biocompatibility and customizability. Current soft electronics predominantly rely on traditional manufacturing approaches (e.g., screen printing[13] and vacuum deposition,[6] etc.) to pattern conductive materials onto elastomeric substrates (e.g., silicone rubbers[14,15] and thermoplastic polyurethane (TPU),[1] etc.). To allow stretchability, circuits and interconnects either adopt rigid materials patterned into serpentine-like geometries[8,16] or intrinsically stretchable conductors.[17,18] Despite significant progresses made in the field, inevitable dissimilarities persist between elastomers (~0.1-1 MPa, dry) and biological tissues (1-10 kPa, high water content), which can lead to multiple immune responses that impede the integration of electronics with organisms.[19] Furthermore, limited by both materials and manufacturing strategies, most current reported soft electronics only allow planar or 2.5D configurations, which severely hinders their compatibilities with the geometry-sensitive biological and bio-inspired applications.

Regarding material choices, hydrogels have recently emerged as an ideal candidate for ultra-soft and stretchable electronics with outstanding bioaffinity.[19–24] A hydrogel is a network of hydrophilic polymers that hold a large amount of water, thus it possesses inherent physicochemical similarities with biological

tissues such as extremely low stiffness and high water content. To enable conductive features within hydrogel matrix, methods such as direct encapsulation of titanium wires[20] and trapping liquid metals in pre-formed microfluidic channels within the hydrogels[21,22] have been reported. In the former case, the use of metallic wires prohibits the patterning of conductive features into complex 3D geometries and integration with other electrical components, while in the latter case, the use of liquid metals can cause leakage issues, particularly at the interconnect positions.[25] To date, the precise patterning of conductive materials within the hydrogel matrix remains challenging, and most existing fabrication methods also rely heavily on manual operation which limits their scalability and repeatability. Therefore, a generalized manufacturing approach with high designability, precision and automation for hydrogel electronics is urgently needed.

Here, we develop a set of new materials, including a hydrogel supporting matrix and a conductive ink, to realize the embedded 3D printing (EM3DP) of functional hydrogel-based 3D electronics. EM3DP takes advantages of freeform, multi-material patternability[26–30] and thus represents an ideal platform for 3D soft electronics fabrication. For the first time, we demonstrate that by directly printing conductive inks and components (via pick-and-place) within a hydrogel supporting matrix that can be cured after printing to encapsulate the circuitries, soft electronics with customizable 3D geometries and functionalities can be precisely produced. To enable the EM3DP of conductive ink and discrete electrical components, our supporting matrix possesses eligible rheological properties and a secondary crosslinking mechanism, which renders it fully curable into an ultra-soft and stretchable hydrogel monoblock after printing. The hydrogel-based conductive ink also displays a high electrical conductivity (~1400 S/cm), high stretchability and excellent adhesion with the surrounding matrix. Several hydrogel-based electrical devices including resistive strain sensors, bending sensor-equipped actuators, and inductors are printed and tested for their functionalities. Discrete electrical components including light emitting diodes (LEDs) and radio frequency identification (RFID) chips are readily incorporated into the circuitries via an automated hybrid printing process to expand the functionalities of the printed electronics. Overall, our EM3DP technology provides a versatile manufacturing platform for hydrogel-based soft electronics.

2. Results And Discussion

2.1. Materials for embedded 3D printing

Our method for formulating the supporting matrix involves the preparation of granular hydrogel microparticles, which exhibits yield stress fluid-like rheological properties.[27-30] When a nozzle moves across the granular hydrogels and causes a shear force that is greater than their yield stress, they will undergo a jamming-unjamming transition and temporarily transform from a solid state to a flowable liquid-like state to accommodate the motion of the nozzle without creating crevices. Upon shear force removal, the temporarily fluidized gel rapidly returns to its jammed solid state, firmly holding the printed ink in place and preventing it from gravity-driven collapse. Different from previous reports on EM3DP where hydrogels are simply used as sacrificial support,[28,29,31] we develop a fully curable hydrogel matrix

by leveraging the orthogonal crosslinking mechanisms of the alginate–PAM double network hydrogel: alginate chains can form ionic crosslinks with Ca^{2+} in aqueous solutions, while the PAM network is formed by the covalent crosslinking of acrylamide and crosslinkers by radical polymerization. Instead of inducing the ionic and covalent crosslinking simultaneously as a one pot reaction,[20,32] we decouple them into two orthogonal processes to allow the precise control of matrix gel rheological properties while maintaining its curability. Specifically, a solution containing acrylamide as monomer, N,N'-methylenebisacrylamide (MBA) as crosslinker, ammonium persulfate (APS) as thermo-initiator and sodium alginate is first formulated and introduced with Ca^{2+} ions to form an alginate–Ca^{2+} hydrogel (**Figure 1a**). This ionically crosslinked gel monoblock is then pulverized, filtered, and degassed to create hydrogel microparticles with an average diameter of ~20 μm, which appears transparent and exhibits a yield stress fluid behavior, thus it can serve as the supporting matrix for EM3DP (**Figure 1b** and **Supplementary Figures 1** and **2**). Besides, the destroyed alginate–Ca^{2+} ionic bond is reported to be almost irreversible at room temperature, but partially recoverable at 60 °C,[33] which guarantees the long shelf life of the matrix gel at low temperature. Note that acrylamide in the formulation could be replaced by other radical polymerizable monomers such as poly(ethylene glycol) diacrylate without affecting printability and curability (**Supplementary Figure 3**).

Equally important for the EM3DP of hydrogel electronics is the conductive ink which allows: i) high resolution 3D printing; ii) high conductivity; iii) curing and formation of a robust interface (preferably via covalent crosslinking) with the surrounding matrix. We next develop a conductive ink by mixing the as-prepared supporting matrix gel with 5-μm sized Ag flakes (**Figure 1a**), as well as glycerol and water-soluble polymer (e.g., PVP) as additives. Using the same base material as the supporting matrix allows the conductive ink to form a seamless covalent crosslinking with the surrounding materials upon curing, while using Ag flakes as the conductive fillers ensures its conductivity, which would permit applications (e.g., wireless energy supplying) usually unachievable by ionically conductive hydrogels with a conductivity normally < 0.1 S/cm.[34] Note that other fillers such as carbon nanotubes can also be employed (**Supplementary Figure 3**). Finally, glycerol functions as a hygroscopic agent to prevent the ink from dehydration, while the water-soluble polymer improves the dispersing homogeneity of the Ag flakes, benefitting the formation of percolative networks and effectively maintains the high conductivity of the printed structures under stretching (**Supplementary Figure 3**).

The EM3DP is carried out on a custom-built direct ink writing (DIW) platform (**Figure 1b**). After printing, the hydrogel is heated at 60 °C to trigger the radical polymerization of PAM, curing the entire matrix and circuitries within (**Figure 1c(i,ii)**). A mild curing temperature of 60 °C is adopted to minimize the occurrence of bubbles, while the alginate–Ca^{2+} ionic bonds can partially recover at such temperature to toughen the cured hydrogel.[33] The cross-sectional SEM image shows that Ag flakes form a percolative pathway in the cured hydrogel (**Figure 1c(iii)**), with no obvious seam observed between the ink and the matrix (**Figure 1c(iv)**), which is critical for avoiding the delamination between the circuits and the matrix upon large deformation. As shown in **Figure 1d**, the cured hydrogel with an embedded circuitry can withstand a large degree of stretching and twisting, and it can completely recover back to its original

shape once stress is removed without damaging or delaminating. To further demonstrate the advantages of EM3DP in fabricating freeform 3D structures, we print a complex 3D pyramid-in-heptadecahedron caged structure (**Figure 1e** and **Supplementary Video 1**). The whole structure is compressed and recovered back to its original shape without damaging, again highlighting the excellent elasticity and the strong coalescence between the conductive ink and the matrix.

2.2. Rheological properties of the supporting matrix and Ag–hydrogel ink

We next optimized the rheological properties of the matrix and the ink. Supporting matrices with varying alginate content all display a shear thinning behavior (**Figure 2a, left**), and the viscosity increased by ~10 times as the alginate content increases from 0.99% to 2.31%. Matrices with a low (0.99%), medium (1.65%) and high (2.31%) alginate content all show higher storage (G') than loss moduli (G'') (**Figure 2a, right**), and both their G' and G'' increase as the alginate concentration increases. Moreover, the matrices display a yield stress increase from 12.1 to 528.1 Pa as the alginate content increases from 0.99% to 2.31%. Consequently, the matrix with 0.99% alginate slowly collapses, whereas the matrices with 1.65% and 2.31% alginate show solid-like behavior (**Figure 2b**). The effect of alginate content on the rheological properties of the matrices might be attributed to the mechanical property change of the alginate–Ca^{2+} hydrogel microparticles. As the alginate concentration increases, more alginate–Ca^{2+} ionic bonds form, leading to higher Young's moduli (**Supplementary Figure 4**), which in turn hinders the relative movement of the hydrogel microparticles. Using the same medium (1.65%) alginate content as the supporting matrix as base material, the addition of Ag flake increases the conductive ink viscosity (**Figure 2c, left**), indicating that Ag flakes also function as a rheological modifier. Compared to the pure matrix gel, the 1.5×Ag ink (Ag/supporting gel mass ratio = 1.5) displays a viscosity increase of roughly an order of magnitude, while the shear thinning behavior remains the same in all inks. The G' and G'' of the inks also show a dramatic 10-fold increase as the Ag/hydrogel ratio increases from 0 to 1.5 (**Figure 2c, right**).

We next performed the EM3DP of 1.5×Ag ink conductive ink within the hydrogel supporting matrices with different alginate contents. The supporting matrix with a medium (1.65%) alginate content displays the most suitable printing condition (**Figure 2b(ii), middle**) and the ink is readily sheared when pneumatic pressure is removed (**Figure 2b(ii), right**), thus it is adopted for the next EM3DP. The low (0.99%) and high (2.31%) alginate content shows non-ideal dragging of the filaments during stop-and-go printing (**Figure 2b(i), right**) and crevasses formation (**Figure 2b(iii)**) after nozzle moves through the matrix, respectively (see SI for more information). By optimizing the printing parameters, including pressure and nozzle moving speed, the printed ink filaments can be precisely controlled to coincide with the inner diameter (ID) of nozzles (**Figure 2d**). All filaments display smooth surfaces without obvious shape change or bubbling during the thermo-curing process.

2.3. Mechanical properties of the cured hydrogel matrix

Once the printing completes, the whole supporting matrix is cured to form an ultra-soft and stretchable hydrogel monoblock. **Figures 3a**,**b** compare the stress–strain curves of the alginate–PAM double network

hydrogels prepared through the conventional one-pot method (non-pulverized) and our method (pulverized), respectively, with a fixed crosslinker/monomer mass ratio and a varying alginate content. For non-pulverized hydrogels, an obvious yielding occurs at ~230% strain, which is not observed for the pulverized hydrogels, likely ascribed to the breakage of the alginate–Ca^{2+} network during the stretching of the non-pulverized hydrogels,[33,35] whereas the alginate–Ca^{2+} network has already been pre-destructed in pulverized hydrogels and unable to recover completely at 60 °C. The non-pulverized hydrogels also display a higher level of relaxation than the pulverized ones (**Supplementary Figure 5**), which can also be attributed to their more abundant alginate–Ca^{2+} bonds. As the alginate content increases from 0.99% to 2.31%, the Young's moduli of the non-pulverized hydrogels show an increase from ~5.35 to ~7.69 kPa, whereas the Young's moduli of the pulverized hydrogels increases from ~2.80 to ~3.71 kPa (**Figure 3c**). While the Young's moduli of the non-pulverized hydrogels were around 2-times higher than their pulverized counterparts, they both exhibit a high ultimate elongation (λ) of ~18 ± 2, indicating that the alginate–Ca^{2+} network had little impact on the stretchability of the hydrogels. Hence, the absence of a strong ionic network can lead to softer hydrogels (< 5 kPa) without affecting their stretchability, which should favor their applications as epidermal or implantable devices.

Compared to alginate content, the crosslinking degree of the hydrogels plays a more significant role on tuning their mechanical properties. As shown in **Figure 3e**, at a fixed alginate content (1.65%), raising the crosslinker/monomer mass ratio of the pulverized hydrogels from 0.016% to 0.082% lead to a slight increase in Young's moduli from ~3.05 to ~3.3 kPa but a great improvement in λ from ~11.3 to ~19.5 (**Figure 3f**). Further increasing the crosslinker/monomer mass ratio to 0.820% dramatically increases the hydrogels' Young's modulus to ~31.8 kPa but reduces their λ to only ~1.54, indicating that by adjusting the crosslinker content, the stiffness of the cured hydrogels can be readily controlled to manufacture hydrogel electronics requiring distinct mechanical properties.

2.4. Electrical performances of the Ag–hydrogel ink and stretchable hydrogel electronics

Blending nano/microscale conductive fillers (e.g., Ag flake[1] and CNT[36]) with stretchable matrix materials (e.g., TPU,[1] PDMS[37] and hydrogel[38]) represents a widely adopted strategy for designing stretchable conductive inks. For example, recently, a conductive hydrogel composite consisting of Ag flakes and alginate–PAM hydrogel has been reported,[38] which shows a good conductivity (up to ~350 S/cm) upon a partial drying process. However, nearly all these composites are prepared by uniformly blending conductive fillers with matrix materials, thus they typically require a high filler content to enable sufficient electrical conductivities. By contrast, conductive composites can also be constructed as a segregated structure with conductive fillers located primarily at the boundaries of polymer domains, therefore dramatically reducing their percolation threshold.[36] This strategy has been previously applied to elastomer-based materials but has not been reported for hydrogels, presumably because of the challenges in introducing a secondary interparticle crosslinking mechanism for the hydrogel granules. Our proposed orthogonal crosslinking mechanism of the supporting matrix renders it a viable approach

for making conductive composite inks with a segregated distribution, as schematically represented in **Figure 1a**.

We next compared Ag–hydrogel composites with random and segregated distribution of Ag flakes in hydrogel. SEM images of the cured composites show that at a same Ag content (1.5×Ag), the sample with randomly dispersed Ag flakes fail to form robust interconnected pathways (**Figure 4a** and **Supplementary Figure 6**). On the contrary, in the segregated composite sample, Ag flakes are mainly confined and densely packed at the boundaries of the hydrogel domains (marked by solid red lines). **Figure 4b** compares the electrical conductivity of the Ag-hydrogel composites, measured using a custom-designed sample holder to avoid dehydration (**Supplementary Figure 7**). For the segregated Ag–hydrogel composites, a drastic increase in electrical conductivity from ~1.5×10^{-3} to 2.1×10^{1} S/cm is achieved when the Ag/hydrogel mass ratio increases from 0 to 50%. The conductivity then increases to ~4.0×10^{2} and ~1.4×10^{3} S/cm as the Ag/hydrogel mass ratio increases to 100% and 150%, respectively, which is higher than any other hydrogel-based composites reported to date. In comparison, the Ag–hydrogel composites with randomly distributed Ag flakes show conductivities of only ~6.9×10^{-3}, ~6.9×10^{1}, and ~3.4×10^{2} S/cm at an Ag/hydrogel mass ratio of 50%, 100% and 150%, respectively. These results share a similar trend with previously reported polymer-based conductive composites,[36] highlighting the superiority of the segregated structure in improving conductivities.

We next characterize the electrical performances of the Ag–hydrogel composites under tensile strain (**Figure 4c**). Linear hydrogel resistors with a line width of 250 μm and a length of 18 mm are fabricated using 0.5×Ag, 1.0×Ag and 1.5×Ag inks, showing an initial R (R_0) of 246.5, 10.9 and 3.7 Ω, respectively (**Figure 4d**). The normalized resistance (R/R_0) of the resistors displays a similar linear response upon stretching up to ~200% regardless of the Ag content. After that, 0.5×Ag resistor shows a steeper R/R_0 increase and failed at a strain of 400%. In comparison, the maximum strains of the 1.0×Ag and 1.5×Ag resistors are ~800% and ~1000%, with R/R_0 of ~13.1 and ~9.07, respectively. Under a slow (~5 mm/s) cyclic tensile test, the R/R_0 of the 1.5×Ag resistor sample at ~300% strain slightly increases from ~2.7 to ~3.1 in the first 50 cycles but remain stable afterwards (**Figure 4e**). Increasing the stretching speed leads to higher R/R_0 values (**Supplementary Figure 8**), which is likely due to the hysteresis behaviors of the hydrogels.

We next choose hydrogel-based pneumatic actuator equipped with a resistive curvature sensor to demonstrate the fabrication of a simple hydrogel-based electrical device. The hydrogel actuator is composed of a bottom layer, a main body featuring distinct mechanical properties (**Figure 3e**), an air inlet, and a curvature sensor at the top (**Figure 4f**). When pressure is applied to inflate the air channel, the actuator bends, and the bending angle of the actuator can be detected by measuring the R change of the curvature sensor (**Figure 4g**). Such hydrogel actuators with position feedback might find potential applications in bio-inspired soft robotics for medical applications. We also envision that our EM3DP technology may open new opportunities in the manufacturing of cyborg organs/tissues in the future when cells and biological hydrogels (e.g., gelatin and hyaluronic acid) are employed.

2.5. Printing of functional hydrogel electronics

To demonstrate the advantages of EM3DP in fabricating functional hydrogel electronics, we print 2D spiral (**Figure 5a, top**) and 3D helical (**Figure 5a, bottom**) inductors with different numbers of turns and diameters (**Supplementary Figure 9**), respectively, that can be used for wireless energy harvesting. At 200 kHz, the inductors display similar inductance (*L*) and *R* values to the corresponding simulation (**Figure 5a**). Integration of the printed passive components with packaged ones would greatly expand the functionalities of hydrogel electronics. Instead of soldering commercial components with metal wires[20] or incorporating them into liquid metal circuits via leads,[21] LEDs as a model component can be simply positioned at the exposed pads of the printed hydrogel inductors to form a complete circuit, which can be powered wirelessly by a transmitting coil (**Supplementary Figure 10**) to light up the LED even under stretching (**Figure 5b** and **Supplementary Video 2**). Packaged components can also be integrated into the hydrogel matrix via hybrid printing. Due to the distinct surface properties of electric components and hydrogel, pristine components can easily detach from hydrogel upon deformation. To circumvent this problem, we treated the components based on a previously reported method[39] to allow the formation of a robust covalent connection between their surfaces and the hydrogel matrix/conductive ink (**Supplementary Figure 11**). Using this hybrid printing procedure, we fabricate a hydrogel RFID device consisting of a commercial RFID chip and an inductor (**Figure 5c, left**). The device can endure large stretching up to ~100% strain without delamination (**Figure 5c, middle**), and can be readily attached to body and detected by a RFID reader (**Figure 5c, right**), which promises its potential application in wearable bioelectronics.

To demonstrate the true 3D printability of both conductive features, as well as the precise positioning and integration of discrete electrical components within hydrogel, we fabricate 3D inductor–LED devices through an automated hybrid printing procedure (**Figure 5d** and **Supplementary Video 3**). A packaged LED is picked up by applying a small negative pressure using a ~610 μm ID nozzle and placed into the supporting matrix gel. Subsequently, a 4-turn helical inductor is printed and connected to the LED electrodes before the whole hydrogel bath is cured. The cured device is placed above a transmitting coil to light up the LED (**Figure 5e, top**). When compressed horizontally, the inductor deforms dramatically from a circular to an elliptical shape, leading to changes in its *L* and magnetic flux, and ultimately a reduction in the voltage generated by the inductor. As a result, the LED extinguishes (**Video S4**), but it lights up again when the compression is removed. A simplified model is established to mathematically analyze the induced voltage generated by the inductors (**Supplementary Figure 12**). When the aspect ratio of the device increases from 1 (original state) to 4 (corresponding to the deformed state in **Figure 5e**), the voltage witnesses a 79% reduction (**Figure 5f**), coinciding with the experimentally observed LED intensity change. In comparison, when a vertical compression is applied on the device, the LED remains lit even at a strain of 60% (**Figure 5e, bottom** and **Supplementary Video 4**). Simulation results evidence that the induced voltage increases by around 16% as the compressive strain increases from 0% to 60%. The printed 3D inductor–LED devices can endure large 3D deformation with strain sensing capabilities, which may find applications in the detection of complex stress conditions in biological systems.

3. Conclusion

We develop an EM3DP technology for the facile and programable manufacturing of ultra-soft and stretchable hydrogel electronics. The supporting matrix is designed by leveraging the orthogonal crosslinking mechanism of the alginate–PAM hydrogels. The matrix displays stress yield fluid-like rheological properties, and it is fully curable following EM3DP into an ultra-soft (<5 kPa) and stretchable ($\lambda \sim 18$) hydrogel monoblock. The conductive ink is prepared by blending Ag flakes with the supporting matrix to form a segregated structure, which leads to a high conductivity of up to ~1400 S/cm and a seamless crosslinking with the matrix upon curing. Hydrogel-based resistive sensors are manufactured, and they can endure a maximum elongation up to ~1000%, which are then used in detecting the bending of a hydrogel actuator. Hydrogel-based inductors are also fabricated, which display similar *R* and *L* values to simulation, highlighting the superior designability of our EM3DP method. Moreover, discrete components (LED and RFID) are readily integrated into the printed circuitries through an automated hybrid printing process onto the surface or even within the hydrogel matrix at any designed location. We demonstrate the printed inductors/antenna integrated with discrete components such as LED devices. These devices can endure large 3D omnidirectional deformation and show corresponding electrical feedbacks. Overall, our EM3DP method provides a versatile and promising platform for the future production of functional and ultra-stretchable hydrogel electronics.

4. Experimental Section

4.1. Materials

Glucono delta-lactone (GDL) is purchased from Rhawn (China). Ethylenediaminetetraacetic acid (EDTA) is purchased from Macklin (China). Calcium chloride, sodium hydroxide and dimethylsilicone oil are purchased from General-Reagent (China). Other chemicals are purchased from Sigma-Aldrich (USA) and used as received if not otherwise mentioned. Ag flake (5 μm) and carbon nanotube are purchased from Shanghai Yao Tian Nano Material Co., Ltd (China). Radio frequency identification devices (RFID) (part number: LXMS31ACNA-011) are purchased from muRata (Japan). RFID detector (915 MHz, RD905UW) is purchase from WYUAN (china). Light emitting diodes (LEDs, part number: ORH-B37A) are purchased from Orient (China).

4.2. Preparation of supporting matrix gel

12.117 g acrylamide and a certain amount of alginate (with a content of 0.99%, 1.32%, 1.65%, 1.98% and 2.31% by weight, **Figure 2**) were dissolved in 82.4 g of deionized H_2O at 45 °C under magnetic stirring. After the powder was fully dissolved, the obtained solution was cooled to room temperature. Then, a certain amount of 2 mg/mL N,N'-methylenebis(acrylamide) (MBA) solution (with a mass ratio of 0.016%, 0.082%, 0.205%, 0.410% or 0.820% to acrylamide, **Figure 3**) was added to the solution. 363 mg ammonium persulfate (APS) powder, 3.24 mL EDTA-$CaCl_2$ solution (0.25 M, pH 8.5) and 1.2 g of D-(+)-

Gluconic acid δ-lactone (GDL) powder were also added to the obtained solution and fully dissolved at room temperature under magnetic stirring. The obtained transparent viscous solution was stored at 4 ℃ for 12 h to allow the gelation of calcium alginate. The obtained calcium alginate gel block was first pulverized using a food pulverizer to obtain an initial matrix gel, which was then refined using syringe filters with a size cut-off of 20 μm to obtain the supporting matrix gel for embedded 3D printing. The obtained gel was degassed using a planetary mixer (Thinky ARE-310, Japan) and stored at 4 ℃ to avoid the polymerization of acrylamide. The schematic description of matrix gel preparation can be found in **Supplementary Figure 1**.

To measure the average size of the hydrogel microparticles, 200 μL of black food coloring (McCormick & Co.) was added to the precursor solution during supporting matrix gel preparation. Next, 100 mg of the stained non-filtrated and filtrated gel samples were diluted in 200 μL distilled water. Then, 100 μL of each diluted sample was mounted on a glass slide, covered with a coverslip, and imaged using an optical microscope (SOPTOP, CX400M). The size of the microparticles was measured using NanoMeasurer software (v. 1.2.0).

4.3. Preparation of conductive Ag–hydrogel ink

To prepare the conductive Ag–hydrogel ink, 1 g of the as-prepared supporting matrix gel was first blended with 50 mg of hydrophilic polymer solution (PVP (45-55 kDa, 30 wt.%) or PEO (90 kDa, 4 wt.%)) and 50 mg of glycerol using a planetary mixer at a speed of 1600 rpm for 1.5 min. Then, a certain amount of Ag flake powder (0.5 g, 1.0 g or 1.5 g) is added to the obtained gel and further mixed together (2000 rpm, 1.5 min) for 3 cycles (the mixture is cooled at 4 ℃ for 3 min between each cycle) to obtain the Ag–hydrogel conductive ink. The ink was then transferred and loaded into a 3cc syringe, and centrifuged at 2000×g for 5 min (neofuge 1600, HealForce, China) to degas. The obtained printable ink was stored at 4 ℃ when not using.

4.4. Rheological characterization

To measure the rheological properties of the supporting matrices and the conductive inks, they were loaded onto a Discovery HR-10 rheometer (TA Instrument Co., Ltd., US) with a 25 mm plane plate at 400 μm separation and 25 ℃. Dimethylsilicone oil was dropped at the edge of the plane plate to prevent the samples from dehydration. Viscosity was measured under flow ramp mode with the shear rate ranging from 0.1 to 200 s^{-1}, while storage (G') and loss (G") moduli were measured under oscillatory mode with a frequency of 1 Hz and an oscillation strain rate ranging from 0.01 to 100 s^{-1}.

4.5. Mechanical characterization

The mechanical properties of the hydrogels were measured using an electronic tensile/compressive testing machine (CTM6050, Xie Qiang Instrument Manufacturing Co., LTD., Shanghai, China) equipped with a S9M/1kg force sensor (HBM, Germany). Specimens were prepared by casting supporting matrix (for pulverized hydrogel samples) or non-crosslinked precursor solution (for non-pulverized hydrogel samples) into 3D printed polylactic acid molds, which were then heated at 60 ℃ to induce the polymerization of PAM. For tensile tests, dumbbell-shaped specimens were designed to have a gauge width of 15 mm, a gauge length of 5 mm, and a thickness of 2 mm, and the deformation speed was set at 20 mm/min. For compressive tests, cylindrical specimens were designed to have a diameter of 10.5 mm and a thickness of 4 mm, and the deformation speed was set at 2 mm/min.

4.6. Embedded 3D printing

The as-prepared supporting matrix gel was homogenized and degassed before printing using a planetary mixer (2000 rpm, 1 min), before casting into a PDMS mold to serve as a support bath. Air bubbles created during casting were removed using a 100 μL pipette. The embedded 3D printing of conductive ink in the supporting gel bath was carried out using a custom-built 3-axis high resolution direct ink writing (DIW) platform equipped with a fluid dispenser (Performus V, EFD Inc, East Providence, RI, USA) to control the ink extrusion. The print path was generated by G-code.

4.7. Fabrication of hydrogel actuator equipped with resistive curvature sensor

The hydrogel actuator is composed of a bottom layer, a main body, an air inlet, and a curvature sensor at the top (**Figure 4f**). To prepare the actuator, a precursor solution containing acrylamide, MBA, APS, alginate and EDTA-$CaCl_2$ was prepared, which was then introduced with GDL (to trigger the slow release of Ca^{2+}) and quickly cast into corresponding molds to form the ionically crosslinked bottom layer and the main body of the actuator. Hydrogel supporting matrix was loaded into the mold for the top layer and a bending sensor was embedded printed within the top layer of the actuator to maximize its *R* change upon bending the actuator.[40] The three layers were assembled via covalent crosslinking by heating them together at ~60 ℃ for 1 h under a humid atmosphere. Specifically, the bottom layer has the highest crosslinker/monomer mass ratio (~0.820%) to give it the greatest Young's modulus, whereas the main body of the actuator has a crosslinker/monomer mass ratio of ~0.410% and an intermediate Young's modulus. The top layer has the lowest crosslinker/monomer mass ratio of ~0.082% and the lowest Young's modulus to minimize its influence on the actuator movement.

4.8. Scanning electron microscopy

The hydrogels and conductive inks were characterized using a scanning electron microscope (SEM) (Gemini450, Zeiss, Germany). To do this, cured hydrogel samples with embedded circuits were frozen at -40 ℃ and subsequently lyophilized for 24 h. Next, the obtained samples were notched and manually broken in cross-sectional pieces. The samples were coated with a 5 nm gold film before characterization. To better observe the segregated distribution of Ag flakes in the conductive ink, pulverized but non-filtrated matrix gel was used to obtain a more obvious segregation.

4.9. Electrical characterization

Conductivity measurement

The conductivity of Ag–hydrogel composites with both random and segregated Ag flake distribution was measured by Van der Pauw method using a Hall effect measurement system (HMS-5000, Ecopia, Korea). Composite samples were loaded in a custom-made sample chamber (6 × 6 × 1 mm) to prevent them from dehydration (**Supplementary Figure 7**). Measurements were conducted at a current of 0.5 mA.

Resistance and inductance measurement

The resistance (*R*) and inductance (*L*) of hydrogel electronic samples were measured using a LCR meter (E4980AL, Keysight, USA). To measure the *R* variation of linear resistor samples under stretching, the samples were mounted on a home-built desktop stretcher with 3D printed clamps. Two copper clamps were used to connect the LCR meter and the samples through printed contacts (**Figure 4c**). R_{dc} of the samples was measured in real time as they were stretched by 10% strain steps (at a speed of 5 mm/s and a gap of 3 s) until a sudden surge in R_{dc} was witnessed, which was considered as the failure point of the resistors. To measure the *R* variation of linear resistor samples under repeated stretching, the R_{dc} of hydrogel resistor samples was measured in real time under 300% strain cycles at a speed of 5, 10 and 15 mm/s for 200 cycles. The *L* and *R* of printed 2D spiral and 3D helical inductors were measured at a frequency of 200 kHz.

Wireless energy harvesting

The wireless energy harvesting ability of the printed inductors was demonstrated using a home-built transmitting device powered by an AC/DC generator (Model 615-3, Trek, USA). The detailed design and working mechanism of the transmitting device can be found in supplementary information (**Supplementary Figure 10**).

Simulation analysis

Electrical simulation analysis was conducted using the COMSOL Multiphysics software (version 5.4a). Frequency domain simulation was carried out by using the magnetic and electric fields (MEF) interface in

the AC/DC module. Detailed simulation setup and parameters can be found in supplementary information.

Declarations

Acknowledgements

The authors thank Hangyu Chen for the assistance with the 3D printers. The authors thank the financial support of this research by the National Natural Science Foundation of China (no. 51905446). The authors thank (Dr. Chao Zhang and Dr. Lin Liu from) Instrumentation and Service Center for Physical Sciences at Westlake University for technical supporting in data acquirement and interpretation.

Author contributions

Y.H. and N.Z. designed the research; Y.H. and Z.Q. fabricated the materials; Y.H., H.C. and Yetian Y. performed the general experiments; Y.H. and Q.Q. conducted electrical analysis and simulation works; Y.H. and Yuan Y. analyzed the data; Y.H. and N.Z. wrote the manuscript; Y.H., Yuan Y. and N.Z. revised the manuscript.

Competing interests

The authors declare no competing interests.

References

1. Valentine, A. D. et al. Hybrid 3D printing of soft electronics. *Adv. Mater.* **29**, 1703817 (2017).
2. Boutry, C. M. et al. Biodegradable and flexible arterial-pulse sensor for the wireless monitoring of blood flow. *Nat. Biomed. Eng.* **3**, 47–57 (2019).
3. Liu, Y. et al. Morphing electronics enable neuromodulation in growing tissue. *Nat. Biotechnol.* **38**, 1031–1036 (2020).
4. Yamagishi, K., Zhou, W., Ching, T., Huang, S. Y. & Hashimoto, M. Ultra-deformable and tissue-adhesive liquid metal antennas with high wireless powering efficiency. *Adv. Mater.* **33**, 2008062 (2021).
5. Lu, D. et al. Bioresorbable, wireless, passive sensors as temporary implants for monitoring regional body temperature. *Adv. Healthc. Mater.* **9**, 2000942 (2020).
6. Chen, Y. et al. Skin-like biosensor system via electrochemical channels for noninvasive blood glucose monitoring. *Sci. Adv.* **3**, e1701629 (2017).
7. Tringides, C. M. et al. Viscoelastic surface electrode arrays to interface with viscoelastic tissues. *Nat. Nanotechnol.* **16**, 1019–1029 (2021).

8. Noh, K. N. et al. Miniaturized, battery-free optofluidic systems with potential for wireless pharmacology and optogenetics. *Small* **14**, 1702479 (2018).
9. Zhang, Y. et al. Battery-free, fully implantable optofluidic cuff system for wireless optogenetic and pharmacological neuromodulation of peripheral nerves. *Sci. Adv.* **5**, eaaw5296 (2019).
10. Yuk, H. et al. 3D printing of conducting polymers. *Nat. Commun.* **11**, 1604 (2020).
11. Choi, Y. S. et al. Stretchable, dynamic covalent polymers for soft, long-lived bioresorbable electronic stimulators designed to facilitate neuromuscular regeneration. *Nat. Commun.* **11**, 5990 (2020).
12. Li, Q. et al. Cyborg organoids: Implantation of nanoelectronics via organogenesis for tissue-wide electrophysiology. *Nano Lett.* **19**, 5781–5789 (2019).
13. Tang, L., Shang, J. & Jiang, X. Multilayered electronic transfer tattoo that can enable the crease amplification effect. *Sci. Adv.* **7**, eabe3778 (2021).
14. Lin, R., Li, Y., Mao, X., Zhou, W. & Liu, R. Hybrid 3D printing all-in-one heterogenous rigidity assemblies for soft electronics. *Adv. Mater. Technol.* **4**, 1900614 (2019).
15. Kim, S. H. et al. Ultrastretchable conductor fabricated on skin-like hydrogel–elastomer hybrid substrates for skin electronics. *Adv. Mater.* **30**, 1800109 (2018).
16. Yeo, W.-H. et al. Multifunctional epidermal electronics printed directly onto the skin. *Adv. Mater.* **25**, 2773–2778 (2013).
17. Wang, Y. et al. A highly stretchable, transparent, and conductive polymer. *Sci. Adv.* **3**, e1602076 (2017).
18. Park, J. et al. Soft, smart contact lenses with integrations of wireless circuits, glucose sensors, and displays. *Sci. Adv.* **4**, eaap9841 (2018).
19. Yuk, H., Lu, B. & Zhao, X. Hydrogel bioelectronics. *Chem. Soc. Rev.* **48**, 1642–1667 (2019).
20. Lin, S. et al. Stretchable hydrogel electronics and devices. *Adv. Mater.* **28**, 4497–4505 (2016).
21. Liu, Y. et al. Ultrastretchable and wireless bioelectronics based on all-hydrogel microfluidics. *Adv. Mater.* **31**, 1902783 (2019).
22. Liu, H. et al. Biofriendly, stretchable, and reusable hydrogel electronics as wearable force sensors. *Small* **14**, 1801711 (2018).
23. Liu, H. et al. Spatially modulated stiffness on hydrogels for soft and stretchable integrated electronics. *Mater. Horiz.* **7**, 203–213 (2020).
24. Xu, C., Ma, B., Yuan, S., Zhao, C. & Liu, H. High-resolution patterning of liquid metal on hydrogel for flexible, stretchable, and self-healing electronics. *Adv. Electron. Mater.* **6**, 1900721 (2020).
25. Zhang, L., Gao, M., Wang, R., Deng, Z. & Gui, L. Stretchable pressure sensor with leakage-free liquid-metal electrodes. *Sensors* **19**, 1316–1331 (2019).
26. Muth, J. T. et al. Embedded 3D printing of strain sensors within highly stretchable elastomers. *Adv. Mater.* **26**, 6307–6312 (2014).
27. Bhattacharjee, T. et al. Writing in the granular gel medium. *Sci. Adv.* **1**, e1500655 (2015).

28. Hinton, T. J. et al. Three-dimensional printing of complex biological structures by freeform reversible embedding of suspended hydrogels. *Sci. Adv.* **1**, e1500758 (2015).
29. Lee, A. et al. 3D bioprinting of collagen to rebuild components of the human heart. *Science* **365**, 482–487 (2019).
30. O'Bryan, C. S. et al. Self-assembled micro-organogels for 3D printing silicone structures. *Sci. Adv.* **3**, e1602800 (2017).
31. Highley, C. B., Rodell, C. B. & Burdick, J. A. Direct 3D printing of shear-thinning hydrogels into self-healing hydrogels. *Adv. Mater.* **27**, 5075–5079 (2015).
32. Luo, G. et al. Freeform, reconfigurable embedded printing of all-aqueous 3D architectures. *Adv. Mater.* **31**, 1904631 (2019).
33. Sun, J.-Y. et al. Highly stretchable and tough hydrogels. *Nature* **489**, 133–136 (2012).
34. Ye, Y., Zhang, Y., Chen, Y., Han, X. & Jiang, F. Cellulose nanofibrils enhanced, strong, stretchable, freezing-tolerant ionic conductive organohydrogel for multi-functional sensors. *Adv. Funct. Mater.* **30**, 2003430 (2020).
35. Du, G. et al. Versatile controlled ion release for synthesis of recoverable hybrid hydrogels with high stretchability and notch-insensitivity. *Chem. Commun.* **51**, 15534–15537 (2015).
36. Huang, Q., Tang, Z., Wang, D., Wu, S. & Guo, B. Engineering segregated structures in a cross-linked elastomeric network enabled by dynamic cross-link reshuffling. *ACS Macro Lett.* **10**, 231–236 (2021).
37. Fassler, A. & Majidi, C. Liquid-phase metal inclusions for a conductive polymer composite. *Adv. Mater.* **27**, 1928–1932 (2015).
38. Ohm, Y. et al. An electrically conductive silver–polyacrylamide–alginate hydrogel composite for soft electronics. *Nat. Electron.* **4**, 185–192 (2021).
39. Yu, Y. et al. Multifunctional "hydrogel skins" on diverse polymers with arbitrary shapes. *Adv. Mater.* **31**, 1807101 (2019).
40. Truby, R. L. et al. Soft somatosensitive actuators via embedded 3D printing. *Adv. Mater.* **30**, 1706383 (2018).

Figures

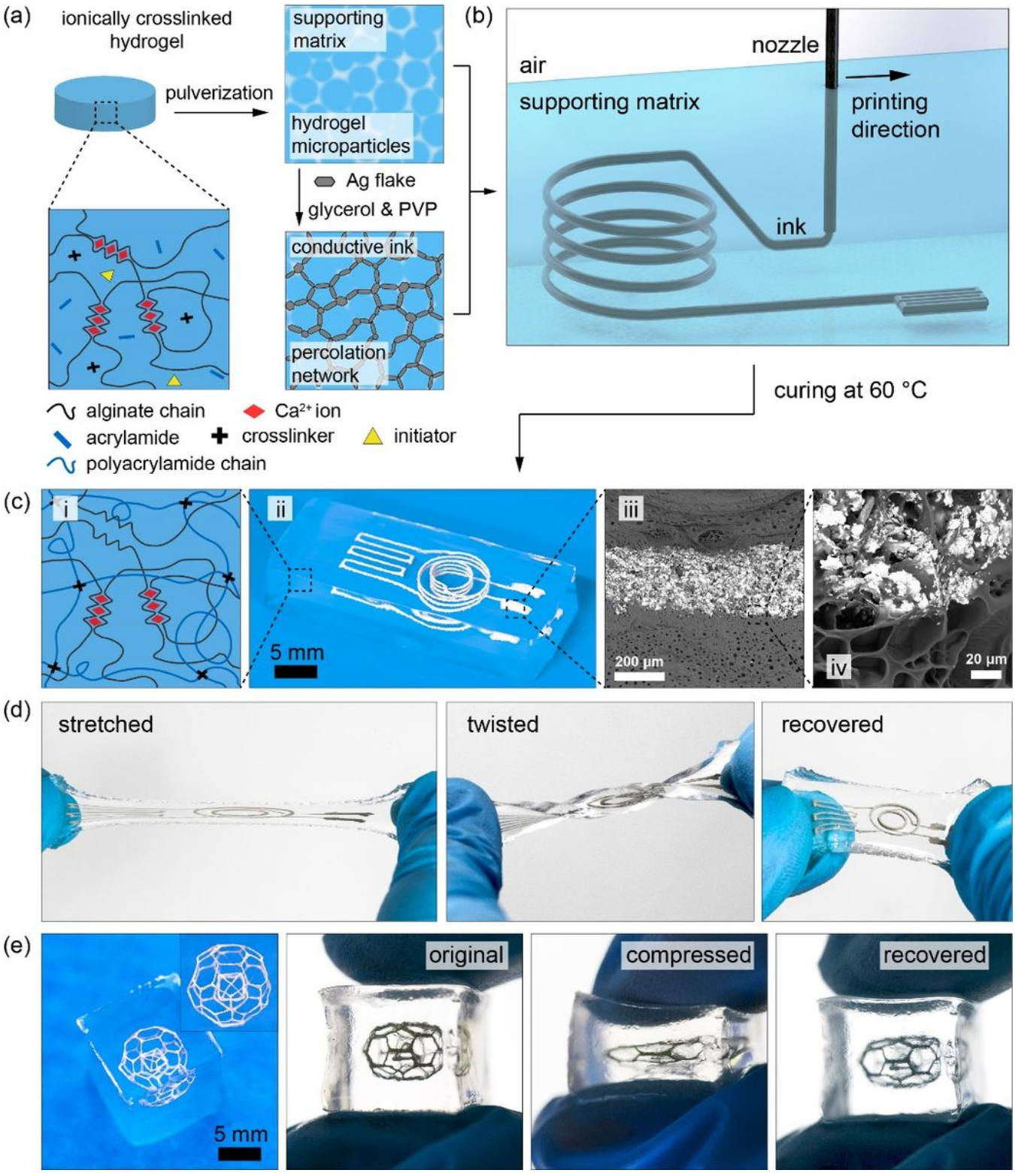

Figure 1

Fabrication of hydrogel electronics via EM3DP. (a) Schematic diagram illustrating the synthetic methodology and chemistry towards formulating the hydrogel supporting matrix and hydrogel-based conductive ink. (b) Schematic illustration of embedded 3D printing of conductive ink into freeform 3D structure within a curable hydrogel supporting matrix. (c) i) PAM forms a covalently crosslinked network by radical polymerization at 60 °C, ii) causing the curing of the hydrogel supporting matrix and printed

circuitries; iii) SEM image showing the Ag flake conductive networks; iv) magnified SEM image showing the interfaces between the conductive ink and the matrix. (d) The cured hydrogel electronic device can undergo large stretching and twisting deformation, but it can recover completely back to their original shape once stress is removed. (e) A complex pyramid-in-heptadecahedron nested conductive structure within a cubic hydrogel matrix is manufactured, compressed, and recovered to its original state.

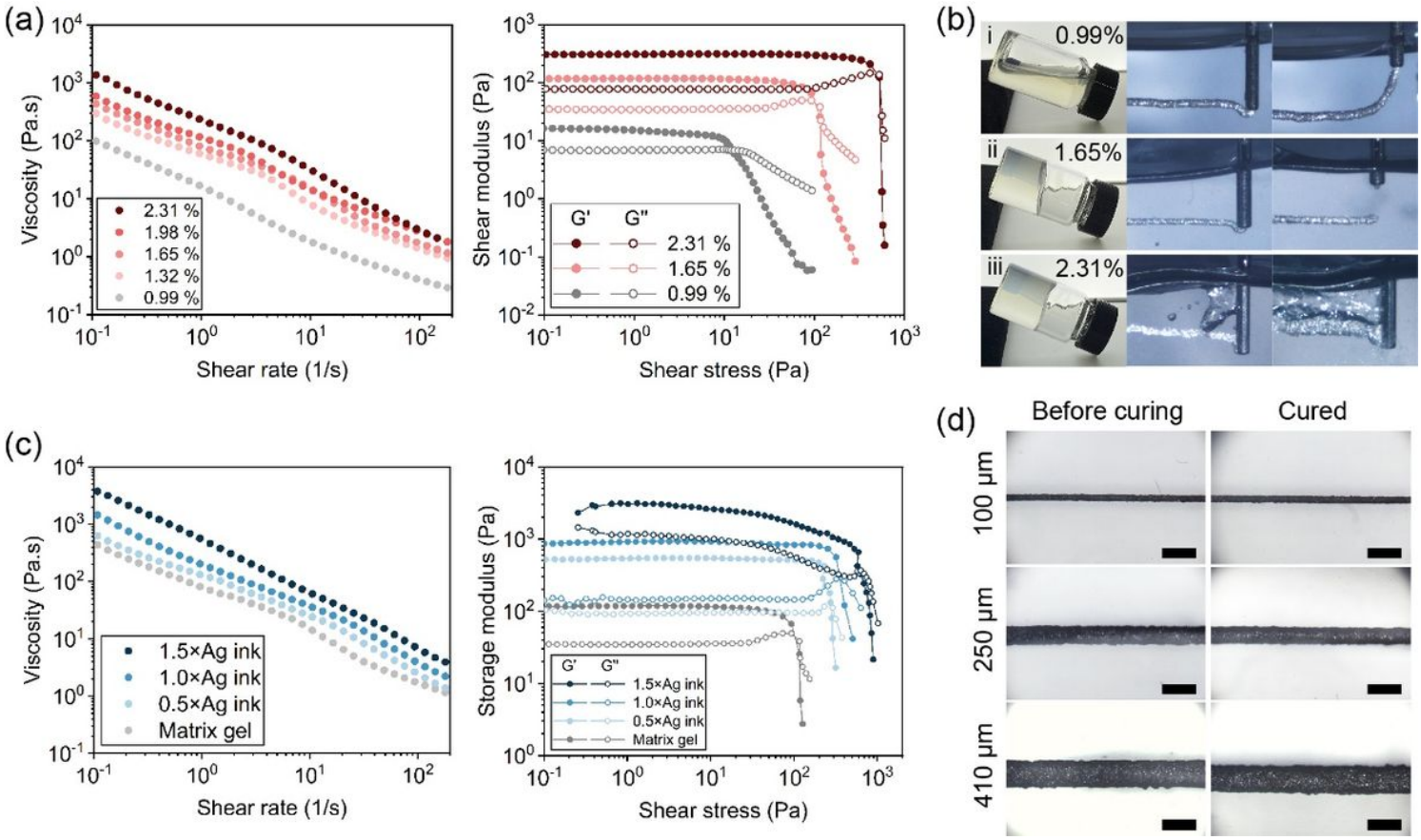

Figure 2

Rheological properties of the supporting matrix and the conductive ink. (a) (left) Viscosity, (right) storage (G') and loss (G'') moduli of the supporting matrices with varying concentration of alginate (0.99%, 1.32%, 1.65%, 1.98% and 2.31% by weight). (b) Suitability of supporting matrices with varying alginate content (0.99%, 1.65% and 2.31%) for EM3DP. (c) (left) Viscosity, (right) G' and G'' of the Ag–hydrogel ink with different Ag/hydrogel mass ratios (0 (Matrix gel), 0.5, 1.0 and 1.5). (d) Optical microscopic images of the Ag–hydrogel ink printed in the supporting matrix using nozzles with different inner diameters (IDs), before and after curing (scale bars = 500 μm).

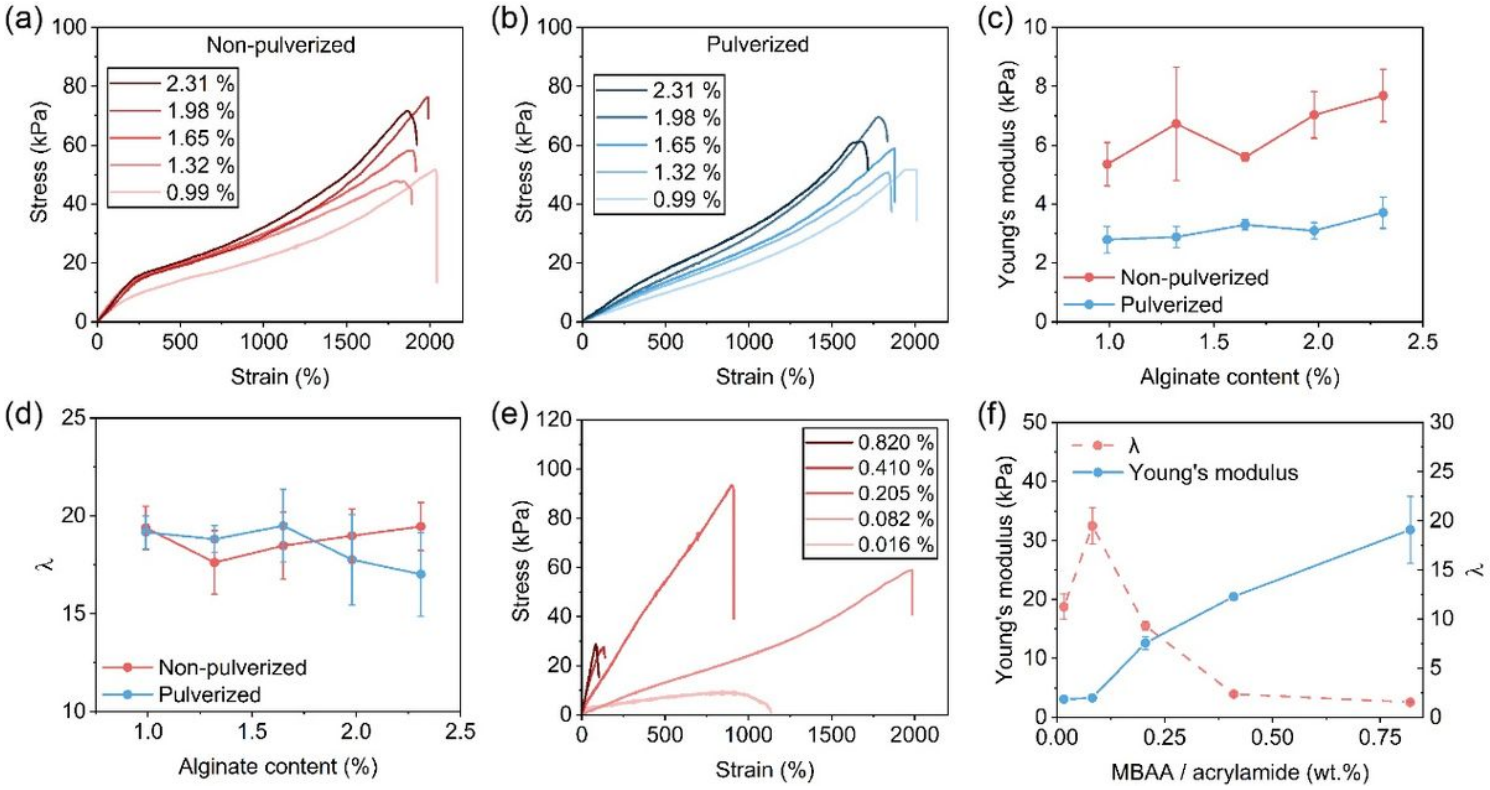

Figure 3

Mechanical properties of cured hydrogel matrices. Stress–strain curves of (a) non-pulverized and (b) pulverized hydrogels with a fixed crosslinker/monomer mass ratio of 0.082% and varying alginate content (0.99%, 1.32%, 1.65%, 1.98% and 2.31% by weight). (c) Young's moduli and (d) ultimate elongation (λ) of the non-pulverized and pulverized hydrogels in (a) and (b). (e) Stress–strain curves of pulverized hydrogels with a fixed alginate content of 1.65% and varied crosslinker/monomer ratio (0.016%, 0.082%, 0.205%, 0.410% and 0.820% by weight). (f) Young's moduli and λ of the hydrogels in (e).

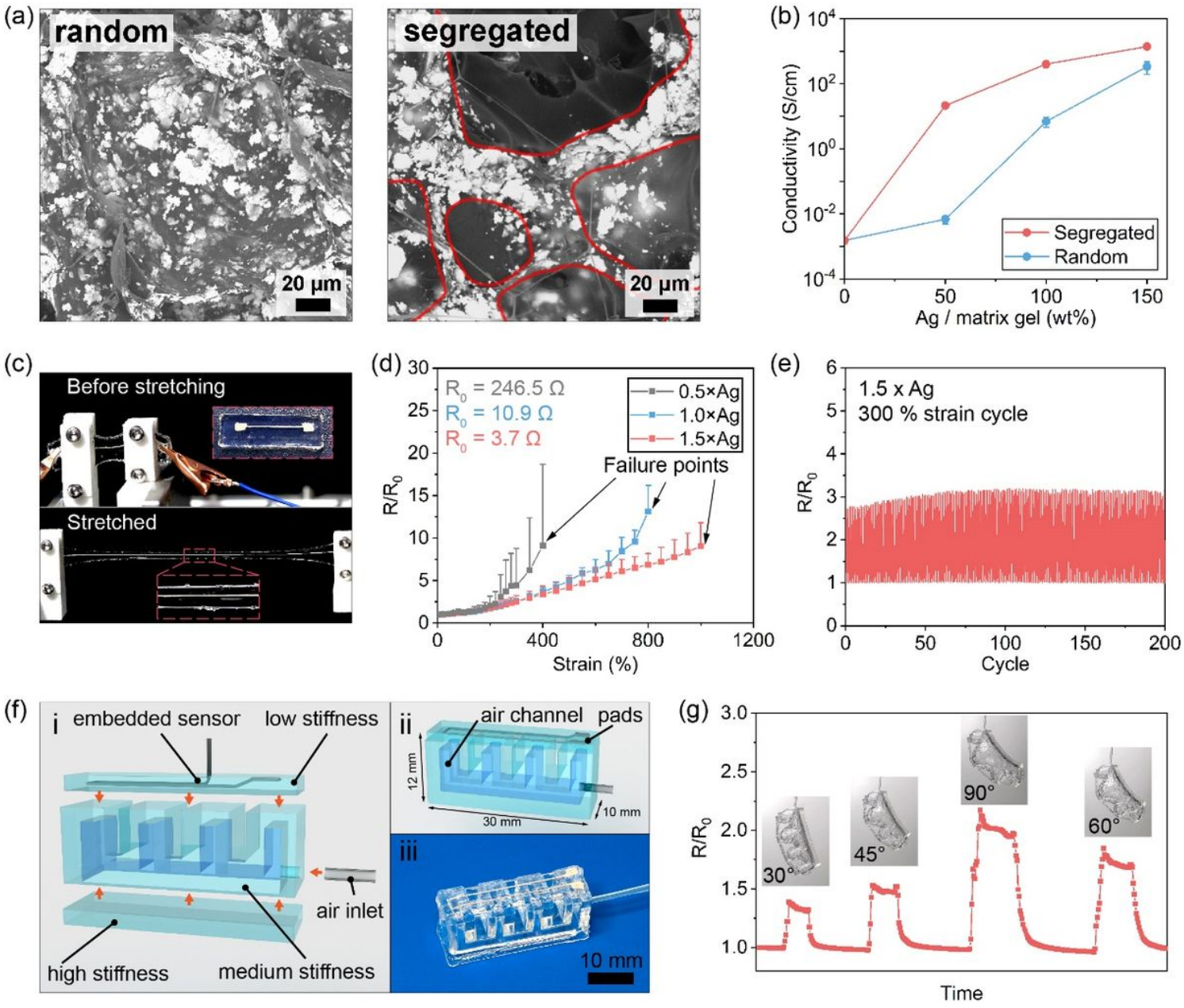

Figure 4

Electrical properties of the Ag–hydrogel ink and demonstrations of printed stretchable hydrogel electronics. (a) SEM images showing the random distribution (left) and segregated distribution (right) of Ag flakes in Ag–hydrogel composites prepared by different methods. (b) Conductivity of the Ag–hydrogel composites with a varying Ag/hydrogel mass ratio (0, 0.5, 1.0 and 1.5). (c) A printed linear resistor sample remains intact under a large stretching deformation. (d) Normalized resistance (R/R_0) of the printed linear resistor samples under stretching, where R is the actual resistance of samples and R_0 is the resistance at 0% strain. (e) R/R_0 of the printed 1.5×Ag linear resistor sample under cyclic stretching (strain = 300%). (f) i) A schematic showing the design of the hydrogel actuator with embedded curvature sensor; ii) schematic and dimensions of the assembled actuator; iii) optical image of the assembled actuator. (g) Curvature sensor characterization of the hydrogel actuator.

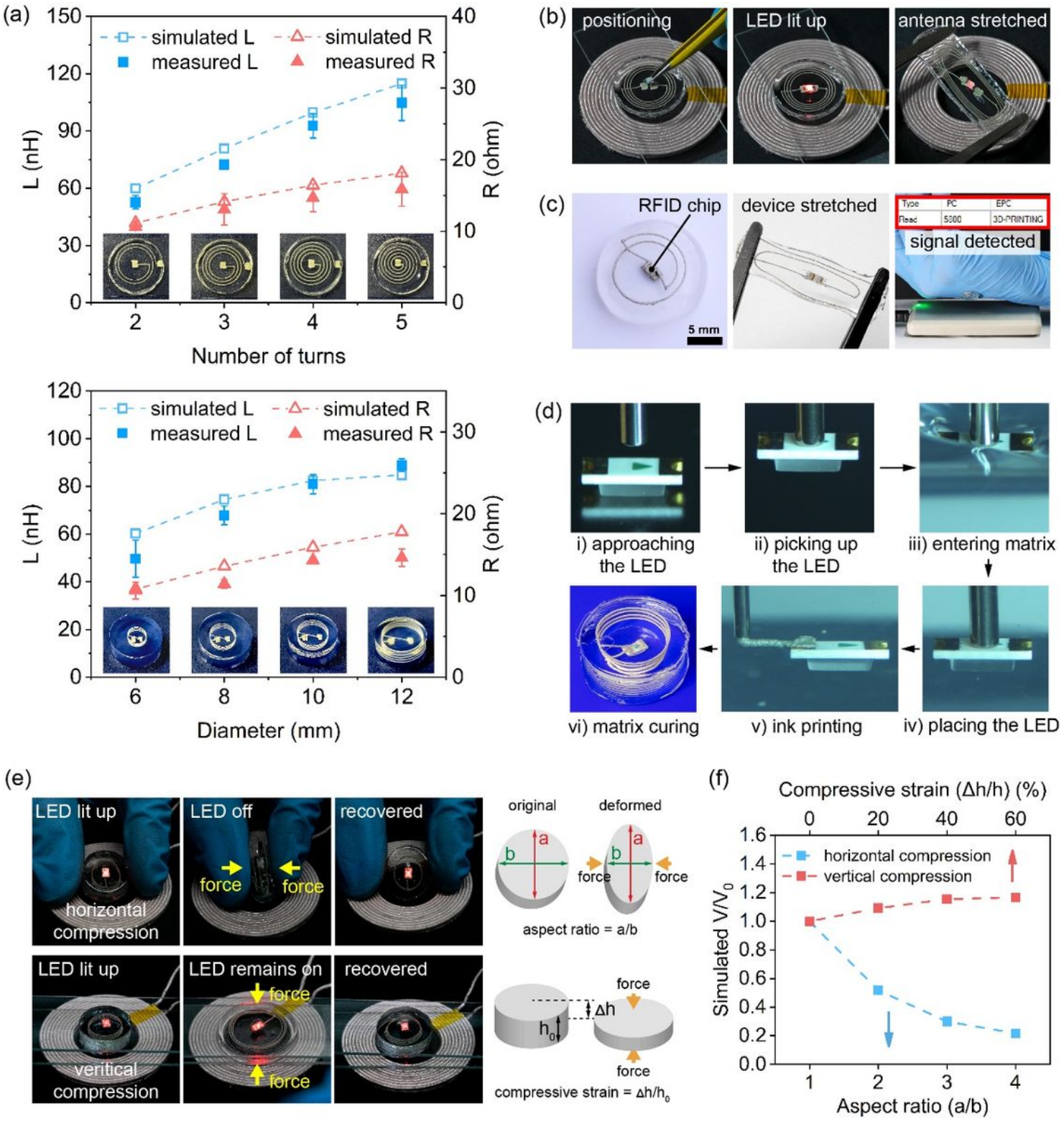

Figure 5

Fabrication of hydrogel electronic devices via hybrid EM3DP. (a) Simulated and experimentally measured inductance (*L*) and *R* values of (top) 2D spiral inductor with varied number of turns (2, 3, 4 and 5) and (bottom) 3D helical inductors with varied diameters (6 mm, 8 mm, 10 mm and 12 mm). (b) LED positioned on a 4-turn 2D spiral inductor is lit up wirelessly. (c) A hydrogel RFID device fabricated by hybrid printing can be detected successfully by a commercial RFID reader. (d) A hydrogel 3D helical

inductor–LED device fabricated via an automated (via a programmable pick-and-place procedure) hybrid printing process. (e) Response of a 3D helical inductor–LED device to (top) horizontal and (bottom) vertical compression. (f) Simulated V/V_0 of a 3D helical inductor under horizontal and vertical compression, where V is the actual voltage generated by the helical inductor, and V_0 is the voltage generated by the helical inductor under no compression.

Supplementary Files

This is a list of supplementary files associated with this preprint. Click to download.

- Supplementaryinformation.docx
- SupplementaryVideo4.mp4
- SupplementaryVideo1.mp4
- SupplementaryVideo2.mp4
- SupplementaryVideo3.mp4